Hind I. Fadhel

Department of Physics, College of Science, University of Baghdad, Baghdad, IRAQ

Synthesis and Characterization of Ag@Cu Core/Shell Nanoparticles via Pulsed Laser Ablation

This study explores the synthesis and characterization of Ag@Cu core/shell NPs through laser ablation in dimethyl sulfoxide (DMSO) and dimethylformamide (DMF) liquids. Employing a Q-switched Nd-YAG laser, we achieved controlled synthesis by directing the laser beam onto pure silver (Ag) and copper (Cu) metal targets immersed in DMSO and DMF, respectively. The two-step ablation method, using Ag nanoparticles as seeds, facilitated the creation of the core/shell structure with varying shell thickness. Detailed characterization was carried out and they provided insights into the optical properties, absorption peaks appear at the wavelength of 350 and 570nm, while the high absorption peak is at the wavelength of 410nm. The crystalline nature and phase composition of Ag was confirmed. The average size is around 30-50nm for Ag in DMF, 55-59nm for Ag@Cu in DMF, 23-70nm for Ag in DMSO and 22-60nm) for Ag@Cu in DMSO.

Keywords: Nanoparticles, Ag@Cu core/shell, Pulsed laser ablation, Nd:YAG laser
Received: 20 January 2024; **Revised:** 02 March 2024; **Accepted:** 09 March 2024

1. Introduction

Nanoparticles (NPs) have become pivotal players in contemporary materials science, exhibiting unique properties and promising applications across diverse fields [1]. Among the myriad of NP architectures, core/shell nanoparticles have garnered substantial attention due to their tunable properties and multifaceted functionalities [2]. The addition of metal ions, such as silver (Ag) and copper (Cu), to glass compositions can modify their physical and chemical properties and provide unique functionality for clinical applications. These metal ions are known to possess antimicrobial properties that can be useful in preventing or controlling infections [3,4]. For instance, silver ions are highly effective against a broad range of microorganisms, including bacteria, viruses, and fungi, by disrupting their cellular processes [5]. There is a high need for antibacterial formulations employed in tissue regeneration therapies [6]. Antibacterial metal ions have been around for a long time [7], and Ag has been shown to have good broad-spectrum bactericidal activity [8].

The utilization of laser ablation as a synthesis technique provides an innovative avenue for the controlled fabrication of nanoparticles. This method offers advantages such as precision, purity, and the ability to tailor the size and morphology of the resulting nanostructures [10]. Investigations focused on the impact of DMSO and DMF, both known for their solvating capabilities [11], in the synthesis of Ag@Cu core/shell NPs. The choice of these liquid media introduces an additional dimension to the synthesis process, allowing us to explore their role in shaping the core/shell architecture.

Figure (1) shows the Ag@Cu core/shell configuration chosen for its inherent synergies between silver (Ag) and copper (Cu). This combination not only enhances the stability of the nanoparticles but also imparts unique properties [12], opening avenues for applications in catalysis, sensing, and beyond. The investigation is centered on the exploration of surface plasmon resonance (SPR) in Ag@Cu core/shell nanoparticles. The collective oscillation of conduction electrons, as exhibited by SPR, governs the optical and electronic characteristics of nanoparticles and is a key determinant in their applications [13].

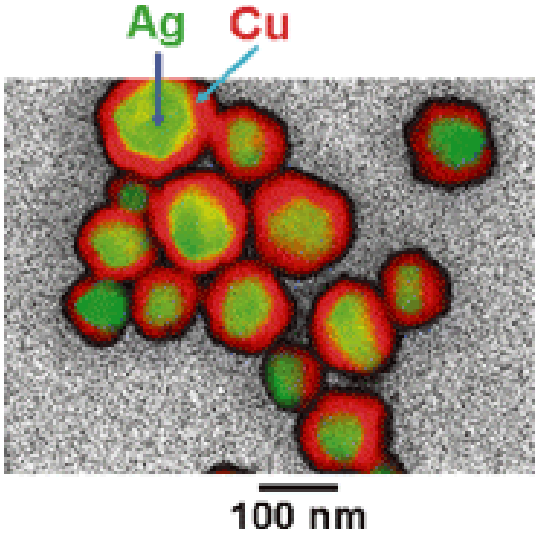

Fig. (1) Ag core-Cu shell nanoparticles [9]

To comprehensively characterize the Ag@Cu core/shell nanoparticles, a series of tests on each sample. UV-visible spectrophotometry analysis was employed to gain insights into the electronic transitions occurring within the nanoparticles, shedding light on their optical properties [14]. The x-ray diffraction (XRD) provided valuable information about the crystal structure and composition, elucidating the structural integrity of the synthesized nanoparticles [15]. Additionally, field-emission scanning electron microscopy (FE-SEM) allowed to introduce the morphology and surface features at the

nanoscale [16], contributing to a holistic understanding of the synthesized Ag@Cu core/shell nanoparticles.

In this study, we delve into the intricacies of synthesizing Ag@Cu core/shell nanoparticles, employing a laser ablation method and using dimethyl sulfoxide (DMSO) and dimethylformamide (DMF) as liquid media. Our exploration of surface plasmon resonance and comprehensive characterization throughout UV-visible spectra, XRD and FE-SEM analyses not only contributes to the fundamental understanding of core/shell nanostructures but also paves the way for their practical applications. By leveraging recent research and insights from the literature.

2. Experimental Part

Monometallic nanoparticles were synthesized utilizing a Q-switched Nd:YAG laser operating at a wavelength of 1064 nm, with a pulse width of 5 ns, and a repetition rate of 6 Hz. The laser beam was directed onto pure (99.9%) metal targets of silver (Ag) and copper (Cu) immersed in two distinct solvents, namely dimethylformamide (DMF) and dimethyl sulfoxide (DMSO). The metal targets were placed within a glass vessel with a total volume of 5 ml. To achieve nanoparticles of varied sizes, the laser energy was set at 1000 mJ using 400 pulses.

A sequential two-step ablation method, schematically depicted in Fig. (2), was employed for the synthesis of bimetallic Ag@Cu core-shell nanoparticles in DMSO and Ag-Cu core-shell nanoparticles in DMF. Initially, a colloidal solution of Ag nanoparticles was prepared by ablating an Ag target in both DMSO and DMF fluids. Subsequently, the Ag target was subjected to laser ablation in the freshly prepared Ag nanoparticle colloidal solution. The Ag nanoparticles served as seeds, forming the core for the ablated Cu species. The ablation process comprised 400 pulses for both Ag and Cu targets to achieve a core-shell morphology.

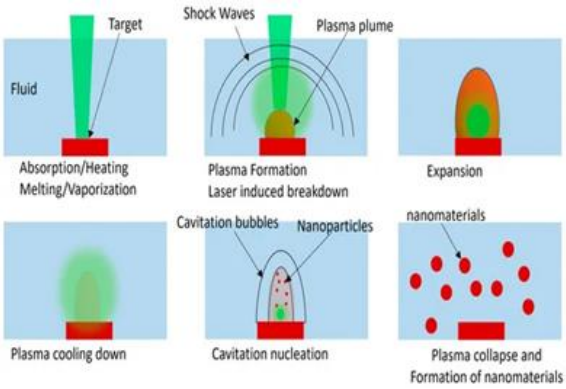

Fig. (2) Schematic illustration of the laser ablation during the laser−target-liquid system for each laser pulse [7]

Optical absorption spectra of the freshly prepared nanoparticles were recorded using a Shimadzu 1800 UV–visible spectrophotometer providing insights into their electronic transitions and optical properties. An AERIS Malvern Panalytical x-ray diffraction (XRD) instrument and Inspect^{tm} F50 FEI field-emission scanning electron microscope (FE-SEM) were used to introduce the structural characteristics of the prepared nanoparticles. The collected nanoparticles were then dried drop by drop onto p-type (100) silicon substrates, preparing them for subsequent XRD and SEM analyses.

This comprehensive experimental approach allowed us to control the size and composition of the monometallic nanoparticles and engineer the morphology of the bimetallic Ag-Cu core-shell nanoparticles. The spectroscopic and structural characterizations undertaken throughout UV–visible, XRD and FE-SEM analyses will provide essential insights into the properties and potential applications of the synthesized nanoparticles. The use of different solvents and the two-step ablation process contribute to the versatility of the proposed synthesis method, offering a platform for tailoring nanoparticle characteristics for specific applications.

3. Results and Discussion

The UV-visible spectra of the synthesized Ag@Cu core/shell nanoparticles revealed distinctive absorption peaks, indicative of the plasmon resonance associated with the nanoparticles.

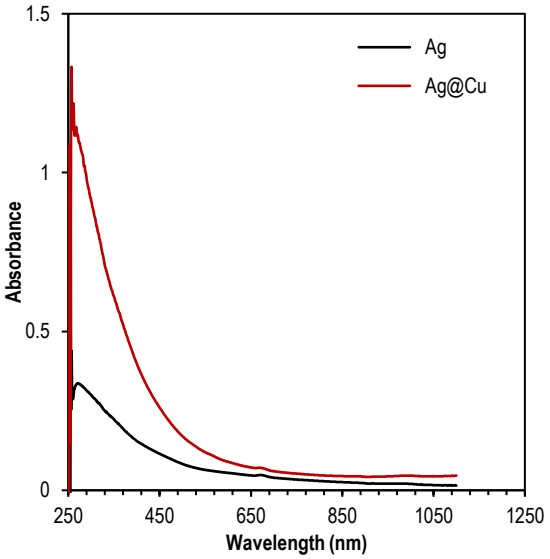

(a) Ag and Ag@Cu in DMF

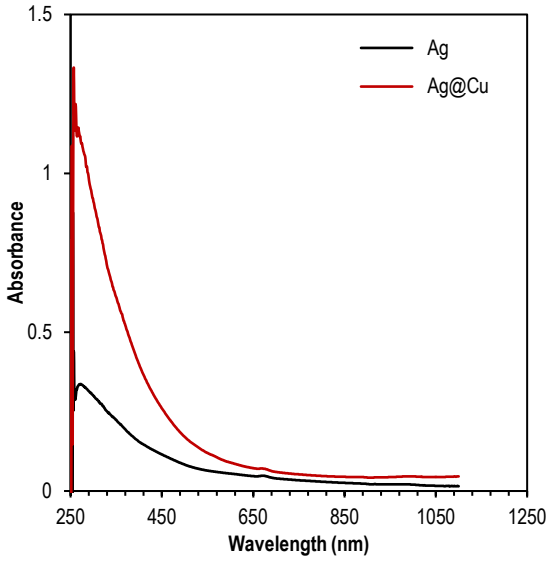

(b) Ag and Ag@Cu in DMSO

Fig. (3) UV-visible spectra for (a) Ag and Ag@Cu in DMF and (b) DMSO

In Fig. (3a), weak absorption peaks appear at the wavelength of 350 and 570nm, while the curve in the same figure shows a relatively high absorption peak at the wavelength of 410nm. This curve is very similar to the curve for silver (Ag). In Fig. (3b), curve no. 1 shows high absorbance in the UV wavelength region, gradually decreasing with increasing wavelength, reaching its lowest value at infrared wavelengths. As for curve no. 2, it shows behavior similar to curve no. 1. With a lower intensity, two absorption peaks appear in this spectrum: the first is high, at a wavelength of approximately 260 nm, while the second peak is centered at a wavelength of approximately 685 nm.

The presence of sulfur (S) within the chemical structure of DMSO solvent led to the formation of the S=O bond [17] and thus increased the polarity of the mixture due to the higher polarity of DMSO solvent compared to DMF solvent (7.2 for DMSO solvent and 6.4 for DMF solvent) as well as the larger value of the dielectric constant (49 for DMSO solvent and 37 for DMF solvent DMF), which caused an increase in the absorption of the mixture in the ultraviolet region (200-400nm), as the dominant spectral activity in this region of the electromagnetic spectrum is due to the $\pi \rightarrow \pi^*$ transitions, which are greatly affected by the polarity of the materials composing the mixture. It is noted that the distinct absorption peak at length The wavelength of 410nm almost disappeared in the case of the mixture in DMF solvent, as the hydrocarbon bonds that make up this solvent are generally characterized by high absorbance in the ultraviolet region of the electromagnetic spectrum.

FE-SEM was employed to unravel the morphological intricacies of the synthesized Ag@Cu core/shell nanoparticles. The obtained images shed light on the structural features, offering valuable insights into the size, shape, and surface characteristics of the nanoparticles.

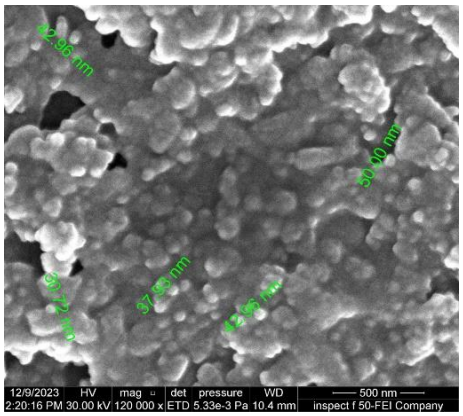

(a) Ag DMF

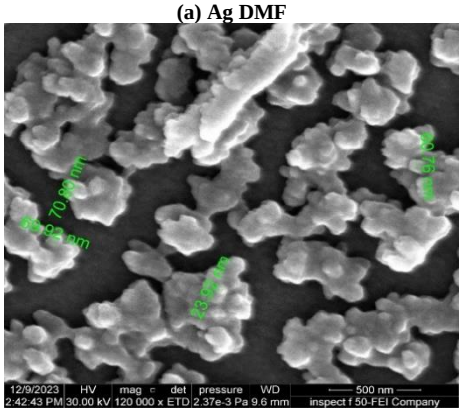

(b) Ag DMSO

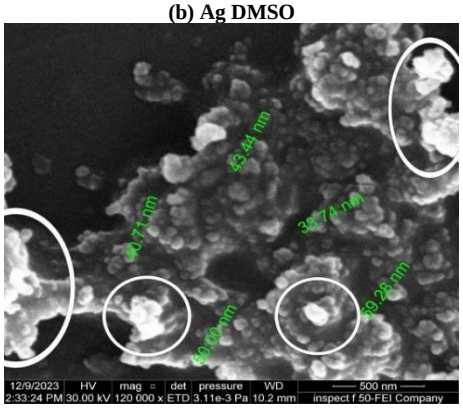

(c) Ag@Cu DMF

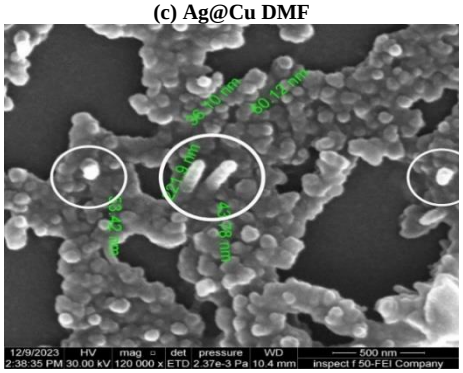

(d) Ag@Cu DMSO

Fig. (4) FE-SEM microimages for (a) Ag in DMF, (b) Ag in DMSO, (c) Ag@Cu in DMF and (d) Ag@Cu in DMSO

In both DMF and DMSO solutions, figure (4) shows that the FE-SEM images revealed well-defined

spherical nanoparticles with a discernible core/shell architecture. The average particle size is around 30-50nm for Ag in DMF and it is more compacted, 23-70nm for Ag in DMSO, and has more aggregation, which means that the same particle size with different solutions, 55-59nm for Ag@Cu in DMF, and 22-60nm for Ag@Cu in DMSO. The colloidal of Ag@Cu core/shell in DMSO is the most homogeneous than the Ag@Cu core/shell in DMF and also has the same particle size with different solutions, and notice that brightness reign shows crystal building, as in figures (4c) and (4d), underscores the precision of the laser ablation technique in controlling particle dimensions [18].

The uniform and spherical morphology observed in the FE-SEM images aligns with the successful formation of Ag@Cu core/shell nanoparticles. This structural integrity is crucial for potential applications in catalysis, sensing, and other nanotechnology domains where specific morphologies are often essential [19]. The distinct core and shell regions observed in the images indicate the effectiveness of the laser ablation process in achieving controlled synthesis [20].

The observed variations in particle size and morphology between DMF and DMSO solutions could be attributed to the solvent influence on nucleation and growth processes during synthesis [21]. DMF, being a polar aprotic solvent, may contribute to different nucleation kinetics compared to DMSO, a highly polar solvent. Such solvent-dependent variations have been noted in recent studies [22].

Additionally, the high-resolution FE-SEM images provide valuable insights into the surface roughness and porosity of the nanoparticles, factors that can influence their catalytic activity [23]. This detailed morphological understanding enhances our comprehension of the structure-property relationships critical for optimizing the performance of Ag@Cu core/shell nanoparticles in diverse applications.

The XRD patterns of Ag@Cu core/shell nanoparticles in DMSO and DMF are characterized by distinct peaks, each corresponding to specific crystallographic planes denoted by the (*hkl*) indices. The (*hkl*) values represent the Miller indices that uniquely identify the crystal planes contributing to the diffraction peaks.

Table (1) XRD peak results for Ag and Ag@Cu in both DMF and DMSO

Ag NPs in DMSO and DMF		Cu NPs in DMSO and DMF	
hkl	2θ	hkl	2θ
(111)	38.10°	(111)	43.47°
(200)	44.37°	(200)	50.37°
(220)	64.17°	(220)	73.99°

The XRD patterns exhibit sharp diffraction peaks, indicative of the crystalline nature of the synthesized nanoparticles. Table (1) illustrates that the corresponding (*hkl*) indices for these peaks can be assigned based on their positions in the XRD spectrum. For Ag, the (111), (200), and (220) peaks agree with the JCPDS card no. (00-001-1167), and for Cu the (111), (200), and (220) peaks in agreement with the JCPDS card no. (00-002-1225). These results signify the predominant crystallographic orientations within the Ag@Cu core/shell nanoparticles.

It can be seen that figure (5a) contains two curves. Seriously, when the XRD analysis subject to the Ag in DMF and Ag in DMSO solutions, at the first moment it has been observed a single crystal with very high-intensity 2θ = 68.80°. When this result was compared with another work, it didn't find the same single crystal, which means that this experiment revealed a novel result that the special peak has 2θ = 68.80° but, to match our results with other works, the XRD pattern has been split into two curves. The top contains concentrated crystalline particles with a high intensity greater than 6400 counts while the bottom has several peaks related to Ag metal obtained using a pulsed laser with low intensity of fewer than 100 accounts have miller indicates by (111), (200), and (220). Figure (5b) shows the result for Ag-DMSO revealed lower intensity (400 counts) compared to the Ag-DMF solution which means that the DMF solution leads to the arrangement of Ag crystals in specific 2θ = 68.80°.

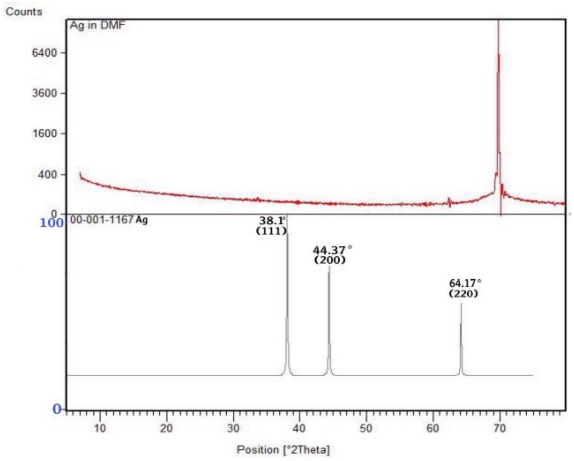

(a) Ag in DMF

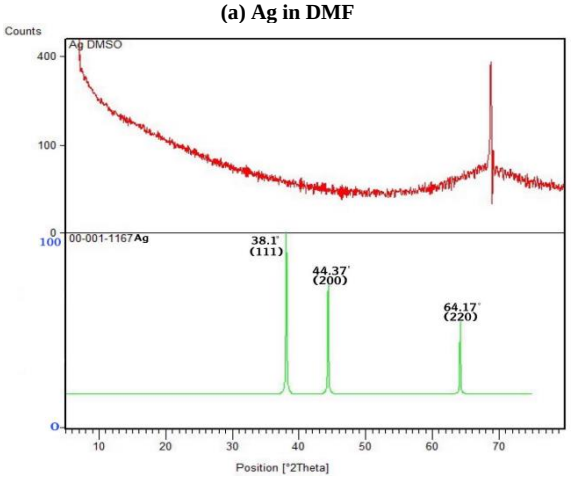

(b) Ag in DMSO

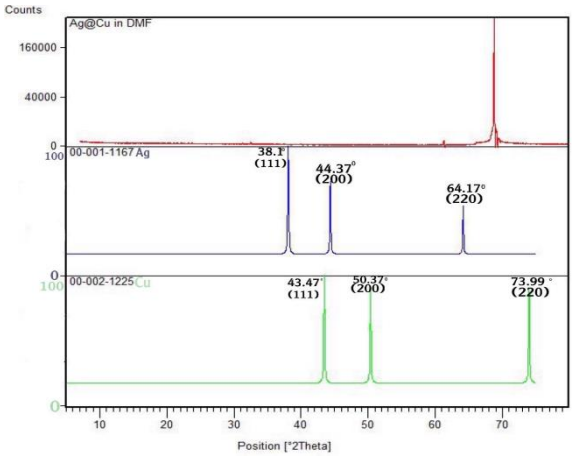

(c) Ag@Cu in DMF

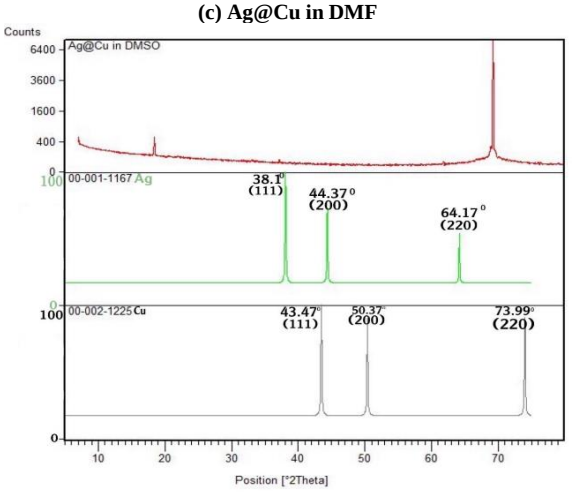

(d) Ag@Cu in DMSO

Fig. (5) XRD results for (a) Ag in DMF, (b) Ag in DMSO, (c) Ag@Cu in DMF and (d) Ag@Cu in DMSO

Figure (5c) demonstrates the incredible outcome analysis of Ag-Cu core/shell in DMF solution produced a very sharp, remarkable, and highest intensity crystal orientation which emphasizes the effect of DMF to conform the order configuration of core/shell, Ag-Cu ordering pattern with the presence of Ag and Cu basis peaks. Figure (5d) illustrates the addition of Cu target in Ag-DMSO solution and application of pulsed laser ablation in the same environment leads to enforcement to produce high intensity (6400 counts) crystal orientation in the same $2\theta = 68.80°$ when comparing with Fig. (5b).

4. Conclusion

The results obtained from this work proved the nanosized core-shell metal NPs with spherical shape. Results also showed that the colloidal of Ag NPs in DMSO is the most aggregation than Ag NPs in DMF, the colloidal of Ag@Cu core/shell in DMSO is the most homogeneous as Ag@Cu core/shell in DMF and has the same particle size with a different solution. The results unveil disparities in the crystalline nature and phase composition of Ag@Cu core/shell NPs. The diffraction patterns exhibit unique peaks (single crystalline) at 2θ=68.80° emphasizing the solvent-driven influence on the formation of the core/shell structure.

References

[1] M. Sajid and J. Płotka-Wasylka, "Nanoparticles: Synthesis, characteristics, and applications in analytical and other sciences", *Microchem. J.*, 154 (2020) 104623.

[2] S. Dhiman et al., "Application of core/shell nanoparticles in smart farming: A paradigm shift for making the agriculture sector more sustainable", *J. Agricul. Food Chem.*, 69(11) (2021) 3267-3283.

[3] A. Mishra, J. Rocherullé and J. Massera, "Ag-doped phosphate bioactive glasses: Thermal, structural and in-vitro dissolution properties," *Biomed. Glass.*, 2(1) (2016) 38-48.

[4] N. Alasvand et al., "Copper/cobalt doped strontium-bioactive glasses for bone tissue engineering applications", *Open Ceram.*, 14 (2023) 100358.

[5] R.H. Hussian and D.K. Mahdi, "Investigation of the Structural Influences of Silver Oxide Addition in the Bioactive Phosphate Glasses", *East Euro. J. Phys.*, (3) (2023) 321-328.

[6] T.A. Kareem and D.K. Mahdi, "Synthesis and characterization of silver nanoparticles-doped mesoporous bioactive glass prepared by spray pyrolysis", *Eurasian Chem. Commun.*, 4 (2022) 330-337.

[7] F.E. Ciraldo et al., "Tackling bioactive glass excessive *in vitro* bioreactivity: Preconditioning approaches for cell culture tests", *Acta Biomater.*, 75 (2018) 3-10.

[8] S. Chernousova and M. Epple, "Silver as Antibacterial Agent: Ion, Nanoparticle, and Metal", *Angewendte Chemie Int. Ed.*, 52(6) (2013) 1636-1653.

[9] M. Tsuji et al., "Synthesis of Ag@ Cu core–shell nanoparticles in high yield using a polyol method", *Chem. Lett.*, 39(4) (2010) 334-336.

[10] M. Alheshibri, "Fabrication of Au–Ag Bimetallic Nanoparticles Using Pulsed Laser Ablation for Medical Applications: A Review", *Nanomater.*, 13(22) (2023) 2940.

[11] V. Vasudevan and S.H. Mushrif, "Insights into the solvation of glucose in water, dimethyl sulfoxide (DMSO), tetrahydrofuran (THF), and N,N-dimethylformamide (DMF) and its possible implications on the conversion of glucose to platform chemicals", *RSC Adv.*, 5(27) (2015) 20756-20763.

[12] K.S. Tan and K.Y. Cheong, "Advances of Ag, Cu, and Ag–Cu alloy nanoparticles synthesized via chemical reduction route", *J. Nanoparticle Res.*, 15 (2013) 1-29.

[13] A. Piatek, "Laser generated magneto-plasmonic Fe-Au Nanoparticles: Formation, Real Structure and Properties", PhD dissertation, Universität Duisburg-Essen (2020).

[14] J. Pansieri et al., "Ultraviolet–visible–near-infrared optical properties of amyloid fibrils shed

light on amyloidogenesis", *Nature Photon.*, 13(7) (2019) 473-479.
[15] R. Schloegl, "X-ray Diffraction: A Basic Tool for Characterization of Solid Catalysts in the Working State", *Adv. Catal.*, 52 (2009) 273-338.
[16] M.A. Majeed Khan et al., "Structural and thermal studies of silver nanoparticles and electrical transport study of their thin films", *Nanoscale Res. Lett.*, 6 (2011) 1-8.
[17] M. Calligaris, "Structure and bonding in metal sulfoxide complexes: an update", *Coordin. Chem. Rev.*, 248(3-4) (2004) 351-375.
[18] T.A. Schmitz et al., "Towards nanoscale molecular analysis at atmospheric pressure by a near-field laser ablation ion trap/time-of-flight mass spectrometer", *Anal. Chem.*, 80(17) (2008) 6537-6544.
[19] F.C. Adams and C. Barbante, "Nanoscience, nanotechnology, and spectrometry", *Spectrochim. Acta B: Atom. Spectro.*, 86 (2013) 3-13.
[20] S. Petrović et al., "Agglomeration in the core-shell structure of CuAg nanoparticles synthesized by the laser ablation of Cu target in aqueous solutions", *J. Opt.*, 17(2) (2015) 025402.
[21] V.A. Ermakov et al., "Size control of silver-core/silica-shell nanoparticles fabricated by laser-ablation-assisted chemical reduction", *Langmuir*, 33(9) (2017) 2257-2262.
[22] D.G. Kwabi et al., "Controlling solution-mediated reaction mechanisms of oxygen reduction using potential and solvent for aprotic lithium–oxygen batteries", *J. Phys. Chem. Lett.*, 7(7) (2016) 1204-1212.
[23] J. Ustarroz et al., "Electrodeposition of highly porous Pt nanoparticles studied by quantitative 3D electron tomography: influence of growth mechanisms and potential cycling on the active surface area", *ACS Appl. Mater. Interfac.*, 9(19) (2017) 16168-16177.

